SCHOLARLY PUBLICATIONS
School of Applied Science
KIIT Deemed to be University

Journal Name: Advanced Materials **IF: 26.8**

Title: Quadruple Moiré Pockets in Lateral Heterobilayers: Programmable Phononic Reconfiguration and Anomalous Second Harmonic Generation

Author: Chakraborty, S.K.; Ray, P.; Sousa, F.B.; Sahoo, C.; Prasad, I.D.; Biswas, S.; Nayak, B.; Kundu, B.; Rojas, R.; Jones, A.J.H.; Miwa, J.A.; Ulstrup, S.; Dutta, S.; Kumar, S.; Malard, L.M.; Pradhan, G.K.; Sahoo, P.K.

Details: November 2025

Abstract: Moiré-engineering in 2D transition-metal dichalcogenides offers access to correlated quantum phenomena. However, simultaneous control over twist-angle (θ) and material combinations to tune phonons, excitons, and their collective interactions remains limited. This study presents scalable, quadruple moiré-pockets formed by vertically stacking chemical vapor deposition-grown monolayer MoS_2–WS_2 and $MoSe_2$–WSe_2 lateral heterostructures with controlled θ (0^o–60°), within a single flatland. Moiré non-rigidity induces lattice-relaxation via rotational reconstruction (θ<8°) and volumetric dilation (θ>8°), resulting in strain-mediated phonon frequency-softening and linewidth-broadening, respectively. Strain localizes selectively in mechanically softer crystal for θ<8°, while an epitaxial-pseudomorphic pattern dominates for θ>8°. Degree of phonon-reconfiguration and angle-resolved photoemission spectroscopy uncover the role of interfacial orbitals in modulating interlayer coupling. At aligned angles (θ–0° and 60°), specifically, MoS_2 exhibits Davydov splitting and reduced valley polarization, reflecting symmetry breaking and chiral phonon effects. At θ–3°, WS_2/WSe_2 shows up to 480% enhancement in second-harmonic generation (SHG), while WS_2/$MoSe_2$ records the lowest due to variations in interlayer-coherence and band-offset-driven phase delay. Notably, at θ–60°, only WS_2/$MoSe_2$ exhibits an anomalous 300% SHG enhancement, attributed to large phase delay and reconstruction-induced strain. Electronic bandstructure calculations support these observations. These findings offer programmable multi-moiré platforms for opto-straintronics, sensing, and on-chip quantum photonics applications.

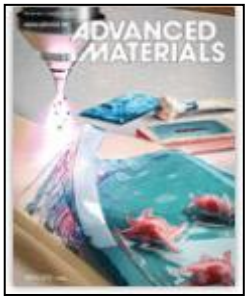

URL: https://advanced.onlinelibrary.wiley.com/doi/10.1002/adma.202520008

SCHOLARLY PUBLICATIONS
School of Applied Sciences
KIIT Deemed to be University

Journal Name: Nature Communications **IF: 14.7**

Title: Evidence of isospin-symmetry violation in high-energy collisions of atomic nuclei

Author: Zwaska R.; Zviagina A.; Zimmerman E.D.; Zherebtsova E.; Zaitsev A.; WyszyÅ„ski O.; WÃ³jcik K.; Witek K.; Wickremasinghe A.; Volkov V.; Vitiuk O.; Vechernin V.V.; VeberiÄ D.; Valiev F.F.; Urbaniak M.; Unger M.; Tveter I.C.; Andronov E.V.; Amin N.; Allison K.K.; Adrich P.; Adhikary H.; Giacosa F.; Gorenstein M.; Poberezhniuk R.; Samanta S.

Details: Volume 16, Issue 1, December 2025

Abstract: Strong interactions preserve an approximate isospin symmetry between up (u) and down (d) quarks, part of the more general flavor symmetry. In the case of K meson production, if this isospin symmetry were exact, it would result in equal numbers of charged (K^+ and K^-) and neutral (K^0 and K^-0) mesons produced in collisions of isospin-symmetric atomic nuclei. Here, we report results on the relative abundance of charged over neutral K meson production in argon and scandium nuclei collisions at a center-of-mass energy of 11.9 GeV per nucleon pair. We find that the production of K^+ and K^- mesons at mid-rapidity is (18.4 ± 6.1)% higher than that of the neutral K mesons. Although with large uncertainties, earlier data on nucleus-nucleus collisions in the collision center-of-mass energy range 2.6<sNN<200 GeV are consistent with the present result. Using well-established models for hadron production, we demonstrate that known isospin-symmetry breaking effects and the initial nuclei containing more neutrons than protons lead only to a small (few percent) deviation of the charged-to-neutral kaon ratio from unity at high energies. Thus, they cannot explain the measurements. The significance of the flavor-symmetry violation beyond the known effects is 4.7σ when the compilation of world data with uncertainties quoted by the experiments is used. New systematic, high-precision measurements and theoretical efforts are needed to establish the origin of the observed large isospin-symmetry breaking.

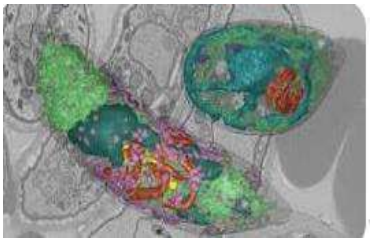

URL: https://www.nature.com/articles/s41467-025-57234-6

SCHOLARLY PUBLICATIONS
School of Applied Sciences
KIIT Deemed to be University

Journal Name: Journal of Energy Storage **IF: 9.8**

Title: Synergistic effect of MoO3@polyindole nanocomposite for high-performance and long-cycle life supercapacitors

Author: Pati, B.; Samal, P.K.; Panigrahy, J.; Praharaj, S.; Rout, D.

Details: Volume 141, Issue 21, January 2026

Abstract: Conducting polymer-based materials have garnered significant attention in energy storage for their wide potential window, high conductivity, substantial capacitance, low cost, and environmental friendliness. This work reports the charge storage performance of MoO_3@PIN nanocomposites (PIN refers to polyindole) for the first time in the literature. The FESEM micrographs of the composites suggest the anchoring of irregular PIN globules on/within the orthorhombic MoO_3 nanobelts, particularly for PM2 (MoO_3:indole::1:2 weight ratio). XPS analysis reveals weak covalent bonds in PM2 via Lewis acidic sites of MoO_3 and nitrogen atoms/ π electrons of pyrrole aromatic rings, facilitating better electron transport pathways within the composite. The above factors contribute to the superior specific capacitance of 631.8 F/g at 1 mV/s over a working potential window of 1.5 V for PM2. It can also deliver an energy density of 103.76 Wh/kg at a power density of 752.28 W/kg, and an impressive cyclic life of 115.5 %, after 14,000 cycles. The PM2//PM2 symmetric cell could achieve an energy density of 28.46 Wh/kg at 600 W/kg and power a red LED for 12 mins. The outstanding cyclic stability, wide potential window, and appropriately balanced energy and power densities of PM2 highlight its potential for supercapacitor electrodes.

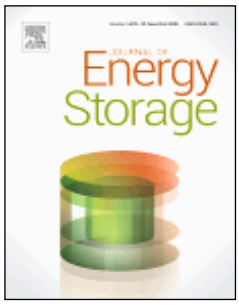

URL: https://www.sciencedirect.com/science/article/pii/S2352152X25039003?via%3Dihub

SCHOLARLY PUBLICATIONS
School of Applied Sciences
KIIT Deemed to be University

Journal Name: Journal of Environmental Chemical Engineering **IF: 7.2**

Title: A comprehensive review on biogenic synthesis and environmental - applications of precious metal nanoparticles

Author: Kar, P; Muduli, S; Nayak, S; Nayak, RK; Parhi, PK

Details: Volume 13, Issue 6, December 2025

Abstract: Water pollution from inorganic and organic contaminants poses a severe environmental and health risk, necessitating the development of sustainable remediation technologies. In recent years, precious metal-based nanoparticles (NPs) have emerged as highly effective materials for pollutant removal from aqueous environments due to their unique physicochemical properties. This review presents a comprehensive overview of the synthesis strategies for precious metal NPs, including physical; laser ablation, ball milling), biological; plant extracts, bacteria, fungi, and chemical; reduction, sol–gel, co-precipitation methods. Unlike previous reviews, this work introduces a comparative framework that systematically links synthesis parameters to na noparticle characteristics and environmental performance. The environmental applications of these NPs—such as adsorption, photocatalytic degradation, catalytic reduction, and antibacterial activity—are critically discussed, with practical examples. For instance, biologically synthesized silver NPs exhibit excellent antibacterial properties and high dye adsorption capacity (up to 161.3 mg/g for Congo red), while gold NPs effectively catalyze the reduction of 4-nitrophenol in pharmaceutical wastewater. The optimization of synthesis conditions and their direct influence on nanoparticle stability, reactivity, and selectivity are thoroughly examined. A variety of advanced characterization techniques used to assess the structural, morphological, and functional attributes of the NPs are also discussed. The influence of synthesis conditions on NP stability, reactivity, and selectivity is examined alongside commonly employed characterization techniques. This review highlights the potential of precious metal NPs as next-generation materials for water treatment, offering insights into their optimization for real-world environmental applications. It also outlines current challenges and future prospects for integrating these nano-materials into scalable and eco-friendly remediation systems.

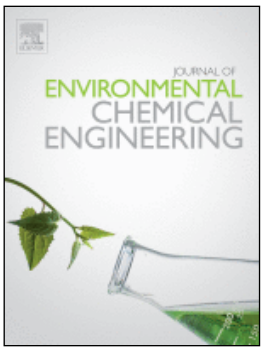

URL: https://www.sciencedirect.com/science/article/abs/pii/S2213343725038606

SCHOLARLY PUBLICATIONS
School of Applied Sciences
KIIT Deemed to be University

Journal Name: Journal of Alloys and Compounds **IF: 6.3**

Title: Correlating dielectric constant and electrical conductivity in NaFeO2: Implications for high- É› electronic device performance

Author: Hota, S.S.; Panda, D.; Choudhary, R.N.P.; Mishra, S.; Biswal, L.

Details: Volume 1047, December 2025

Abstract: $NaFeO_2$ layered oxide was synthesized through the high-temperature solid-state method. The XRD diffraction shows that it has an orthorhombic structure (a = 5.6719 Å, b = 7.1375 Å, and c = 5.3829 Å). The W–H plot was used to obtain the crystallite size, which is determined as 97.9 nm and microstrain is ∼0.0004. Cross-section FESEM image exhibited the uniformity of the grain structure, and the mean grain size can be determined as 1.0457 µm. Temperature and frequency response dielectric studies demonstrated Maxwell-interfacial Wagner's polarization and observed with high dielectric (ε_r∼1218.69) & low dielectric loss (∼4.2) at low frequency. AC conductivity also reinforces low-frequency loss obeying Jonscher's power law. It suggests that the conduction is occurring by a long-range hopping mechanism, and the activation energies were in the range of 0.144–0.259. A change in the power law exponent indicated that OLPT and CBH models may explain the conduction mechanism. Temperature-dependent impedance spectroscopy demonstrated a non-Debye-type relaxation process involving a negative temperature coefficient of resistance (NTCR) behavior having sensitivity 2838.78 and temperature coefficient −1.2 %. The activation energies from both methods indicated different charge carriers involved in the conduction and relaxation processes. This multifunctional material provides a thorough approach to engineering high-performance and promising avenues into future technologies, such as non-volatile memory and spintronic devices.

URL: https://www.sciencedirect.com/science/article/pii/S0925838825065582?via%3Dihub

Journal Name: Biomass and Bioenergy **IF: 5.8**

Title: Sustainable biochar production from shrimp pond algal waste: Optimization of pyrolysis parameters using the L9 Taguchi method

Author: S.P., Palai, Shusree Prachi; S., Senapati, Soumyaranjan; S., Muduli, Sthitiprajna; A.K., Panda, Alok Kumar; T.K., Bastia, Tapan Kumar; P.K., Parhi, Pankaj Kumar

Details: Volume 204, Jan 2026

Abstract: Algal blooms *(Spirogyra)*, a common environmental challenge in shrimp farming, offer a valuable opportunity for sustainable waste conversion into biochar. This study evaluates the feasibility of producing biochar from algal biomass through pyrolysis, focusing on optimizing three key process parameters: temperature, residence time, and heating rate. An L9 Taguchi orthogonal array was used to design the experiments. Biochar yield and quality were analyzed using advanced characterization techniques, including PXRD, FESEM, EDAX, CHNS, RAMAN, FTIR, BET, XPS, analysis, particle density, and pH measurement, to understand the physicochemical properties of the resulting biochar. From the characterization data, the optimization of biochar yield in the context of the functional group's perspective and surface area is 70.5 % and 66.1 %, respectively. The pyrolyzed product, pristine biochar, demonstrated that processing conditions significantly influence biochar structure and properties quantitatively and qualitatively. These findings provide insight into optimal pyrolysis parameters for enhancing biochar quality, with potential applications in environmental remediation and agricultural sustainability.

URL: https://www.sciencedirect.com/science/article/pii/S0961953425008128?via%3Dihub

SCHOLARLY PUBLICATIONS
School of Applied Sciences
KIIT Deemed to be University

Journal Name: Ceramics International **IF: 5.6**

Title: Unraveling the functional behavior of K0.5Bi0.5BaTi2O6ceramic: Structural, optical, dielectric, and electrical aspects for industrial applications

Author: Rout, S.; Priyadarshini, L.; Moharana, K.; Parida, A.K.; Choudhary, R.N.P.; Biswal, L.

Details: Volume 51, Issue 27, November 2025

Abstract: Introducing controlled A-site disorder in double perovskites offers a promising route to tune their physical properties. In this work, Ba^{2+}, $K^{+}$and Bi^{3+}were incorporated at the A-site to modify the structural, optical, dielectric and electrical behaviors. An alkali based disordered novel perovskite solid solution $K_{0.5}Bi_{0.5}BaTi_2O_6$is synthesized using high temperature solid state reaction kinetics. Structural analysis using X-ray diffraction (XRD) and Raman analysis confirmed the solid solution adopt a tetragonal system with a non-centro-symmetric space group P4mm, while energy-dispersive X-ray spectroscopy (EDX) verified the presence and proportion of constituent elements. Optical characterization by UV–Vis spectroscopy established a direct band gap of 3.14 eV, Urbach energy 0.26 eV and a static refractive index of 1.04 endorsing its potential for optoelectronic, photovoltaic and photocatalytic applications. Complex impedance spectroscopy (CIS) demonstrated a high, stable dielectric constant with minimal loss up to 300 °C, while temperature-dependent dielectric analysis indicated a diffuse phase transition (γ = 1.72), confirming the relaxor ferroelectric nature of the material. The material exhibits a high dielectric constant (ε_r∼1467) with a low loss factor (∼0.8) near room temperature (1 kHz). Polarization hysteresis (P–E) loops recorded at ambient temperature yielded a recoverable energy storage density of ∼518.2 J/cm^{3}with an efficiency of ∼43 %. Impedance and conductivity analysis revealed negative temperature coefficient of resistance (NTCR) behavior with intra-grain conduction, applicable for thermistors. AC conductivity followed Jonscher's power law, with charge transport governed by the overlapping large polaron tunneling (OLPT) model. Overall, comprehensive structural, optical, dielectric and electrical characterization demonstrate its multifunctional potential in the field of high-frequency and high-temperature electronics, energy storage and thermistor applications.

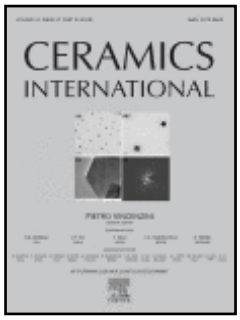

URL: https://www.sciencedirect.com/science/article/pii/S0272884225044189?via%3Dihub

Journal Name: Journal of Physics and Chemistry of Solids **IF: 4.9**

Title: Unveiling the metal-insulator-transition in NaIrO3: The role of spin-orbit coupling and strong electron correlation using ab initio method

Author: Behera, SS; Parida, P

Details: Volume 208, Jan 2026

Abstract: Motivated by the unsuccessful attempts using the density functional theory (DFT) alone to study the insulating behavior of NaIrO post-perovskite compound, employing the interplay between the spin–orbit coupling (SOC) and strong electron correlation (U) effect, we have studied the structural, elastic, and electronic properties of this compound. Here, we have compared the effects of weak Jahn-Teller distortion, strong electron correlation at the transition metal and ligand sites, as well as the spin–orbit effect of the Ir atom to explore the insulating behavior of NaIrO. This post-perovskite compound is associated with the tilting of octahedra in alternate layers, and the ab initio parameters are obtained to carry out this work. We employ the GGA+PBE approximation with full relativistic pseudopotentials to perform calculations including U and spin–orbit interactions within the Quantum Espresso package. From the elastic properties we have investigated that this compound is mechanically stable and ductile in nature. The compound also show anisotropic behavior at different plane.

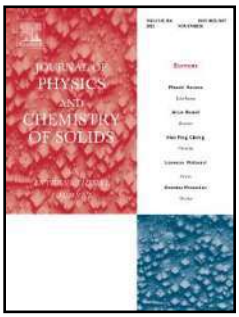

URL: https://www.sciencedirect.com/science/article/pii/S0022369725004615?via%3Dihub

Journal Name: Journal of Physics and Chemistry of Solids **IF: 4.9**

Title: Enhanced magnetic properties and room temperature magnetodielectric response in (1-x) Bi2Fe4O9 - (x) La067Sr033MnO3 (x=0.1-0.3) composites

Author: Pati, A; Mohapatra, SR; Kaushik, SD; Dhara, S; Sahu, DP; Singh, AK; Nanda, J; Tripathy, SN

Details: Volume 208, Issue 2, January 2026

Abstract: We report an enhanced magnetic and magnetodielectric (MD) coupling in antiferromagnetic (AFM) spin frustrated Bi2Fe4O9 (BFO) turned composite with substantial variation of La067Sr033MnO3 (LSMO). Phase formation is confirmed from room temperature Rietveld refinement of X-ray diffraction data. The composite shows orthorhombic crystal structure with space-group 'Pbam + Pbnm' which is also well supported from Raman spectra. XPS analysis confirmed the existence of multiple valence states of magnetic ions such as Fe2+:Fe3+:Fe4+ = 41:45:14 and Mn3+:Mn4+ = 88:12, within experimental limit. This triggers super-exchange and double-exchange interactions thereby contributing significantly to the dielectric and magnetic order parameters. At the same time, with increase in LSMO content an increase in AFM transition temperature (T-N) close to room temperature is observed. An irreversibility in ZFC-FC data is evidenced for T < 350 K along with an opening in M - H plot, indicating spin-glass behaviour and an onset of weak ferromagnetism in the composites. The latter is found to get enhanced significantly with increase in LSMO content and is also verified from Arrott plots. Further, confirmation to the intrinsic MD coupling is assisted by temperature and magnetic field variation of magnetodielectric effect (MD%) which shows enhanced MD effect effective at room temperature. This intriguing MD coupling could be attributed to inverse Dzyalonshinskii-Moriya interactions between magnetic ions present in the composite due to strong cross coupling. Lastly, from Landau free energy expression, the existence of biquadratic nature of magnetoelectric coupling ((PM2)-M-2) emerging from the coupling term 'gamma(PM2)-M-2' is established. At 300 K, gamma is similar to 1.6 x 10(-2) (emu/g)(-2) for BL70-30 and shows similar to 2 % MD response - a nearly eight-fold increase as compared to parent BFO. Hence, the above outcomes highlight the significance of the composite as a viable candidate for multifunctional applications

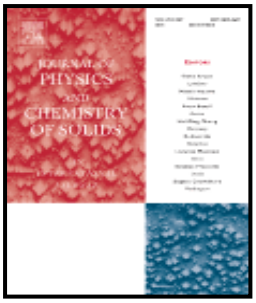

URL: https://www.sciencedirect.com/science/article/pii/S0022369725006122?via%3Dihub

SCHOLARLY PUBLICATIONS
School of Applied Sciences
KIIT Deemed to be University

Journal Name: Journal of Physics and Chemistry of Solids **IF: 4.9**

Title: Probing lattice anharmonicity and thermal transport in nanocrystalline CoSb3 using Raman scattering

Author: A., Mohanty, Abhipsa; A., Das, Arpita; P.K., Deheri, Pratap Kumar; J., Khatei, Jayakrishna; D., Rout, Dibyaranjan; G.K., Pradhan, Gopal K.

Details: Volume 208, January 2026

Abstract: Understanding and controlling thermal conductivity is central to the development of high-performance thermoelectric materials. In this work, we investigate the lattice dynamics and thermal transport in nanocrystalline $CoSb_3$ using non-contact, optothermal Raman spectroscopy. Temperature- and laser power-dependent Raman measurements are employed to analyze phonon dynamics and extract anharmonic contributions from both three-phonon and four-phonon scattering processes. The temperature-induced redshifts of Raman-active phonon modes are modelled quantitatively using the Klemens-Balkanski formalism, incorporating both quasiharmonic thermal expansion and intrinsic anharmonicity. By evaluating the shift in Raman mode positions with respect to laser power and temperature, we estimate the lattice thermal conductivity of nanocrystalline $CoSb_3$ yielding a value of 2.65 ± 0.08 W/mK highlighting strong phonon scattering and thermal boundary resistance at grain interfaces. Our findings underscore the effectiveness of Raman spectroscopy as an analytical technique for probing localized phonon-mediated heat conduction in nanostructured thermoelectrics and offer valuable insights into the role of anharmonic phonon dynamics in determining thermal transport in skutterudites.

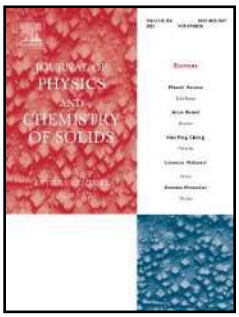

URL: https://www.sciencedirect.com/science/article/pii/S0022369725005815?via%3Dihub

SCHOLARLY PUBLICATIONS
School of Applied Sciences
KIIT Deemed to be University

Journal Name: Journal of Physics and Chemistry of Solids **IF: 4.9**

Title: Unlocking the potential of NiO@BiFeO3 nanocomposite for high-performance supercapacitor electrodes

Author: Rout, S.K.; Samal, P.K.; Panigrahy, J.; Nanda, P.; Pati, B.; Praharaj, S.; Rout, D.

Details: Volume 210, March, 2026

Abstract: The pursuit of electrochemical supercapacitors offering superior energy and power densities has necessitated intensive research into efficient electrode materials. This study explores the potential of NiO@$BiFeO_3$ nanocomposite series as an electrode material. X-ray diffraction confirms the formation of nanocomposites with $Bi_2Fe_4O_9$ as a minor phase, and Rietveld refinement determines their phase percentages. In a three-electrode setup, BN50 (50 wt% $BiFeO_3$ + 50 wt% NiO) demonstrates an excellent specific capacitance of 772 F g^{-1} (at 1 mV/s) and a discharge time of 1080 s (at 0.5 A g^{-1}) from −0.3 to +0.8 V. It is related to the abundance of oxygen vacancies and the existence of multiple oxidation states (XPS), well-interconnected network of irregular particles with minimal agglomerations (FESEM) and synergistic effect of the components in BN50 compared to $BiFeO_3$. A remarkable capacity retention of 120 % is sustained over 20,000 cycles in BN50. Moreover, BN50//BN50 symmetric device exhibits a specific capacitance of 141.68 F g^{-1} at 5 mV/s and delivers an energy density of 28 W h/kg at a power density of 375 W/kg. Two such symmetric cells (series) could power a red LED (1.8 V) up to 10 min. Overall, this work highlights the suitability of NiO@$BiFeO_3$ as a highly redox-active electrode material for charge storage.

URL: https://www.sciencedirect.com/science/article/pii/S0022369725007838?via%3Dihub

SCHOLARLY PUBLICATIONS
School of Applied Science
KIIT Deemed to be University

Journal Name: ACS Applied Electronic Materials **IF: 4.7**

Title: Frequency-Selective EMI Shielding Using PVDF/NiFe2O4//PVDF/Graphene Layered Structure

Author: Samal, PK; Sahoo, R; Dasila, S; Odampilly, RM; Venkatachalam, S; Praharaj, S; Rout, D

Details: Volume 7, Issue 24, December 2025

Abstract: The increasing complexity of our electromagnetic environment is driving a growing demand for flexible, frequency-selective electromagnetic interference (EMI) shielding materials. Herein, we adopt a simple and cost-effective approach to fabricating layered structures consisting of a conducting (7 mL graphene nanoplatelet-coated PVDF) layer and a magnetic (NiFe2O4-coated PVDF) layer. In this sample series, the composition of the conducting layer is fixed while the concentration of NiFe2O4 ink increases from 5 to 40 mL in the magnetic layer. The EMI shielding properties of these layered structures largely hinge on the thickness of the magnetic layer, resulting in a distinctive frequency selectivity. The shielding efficiency for absorption far exceeds reflection (<= 5 dB) at the resonant frequencies, 9 and 11.3 GHz, for all samples. Consequently, the total shielding efficiency (SE T) also peaks at the resonant frequencies. It attains a robust value of 53 dB at 9 GHz and 30 dB at 11.3 GHz for the layered structure containing 10 mL NiFe2O4-coated PVDF (L-NF10). The shielding results are further validated using COMSOL Multiphysics RF module. It also predicts the electric and magnetic field distribution in L-NF10 and electromagnetic power dissipation within each layer. This study introduces an effective strategy for developing layered structures with promising frequency-selective EMI shielding behavior that can be extended to multilayer films by simply modulating the number and order of layers.

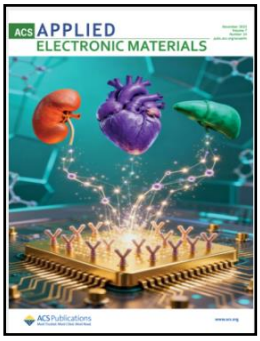

URL: https://pubs.acs.org/doi/10.1021/acsaelm.5c01816

SCHOLARLY PUBLICATIONS
School of Applied Science
KIIT Deemed to be University

Journal Name: RSC Advances **IF: 4.6**

Title: Antibacterial and antibiofilm activity of green synthesized Mg-doped CeO2nanoparticles using Actinidia deliciosa peel extract

Author: Nayak, N.; Suryakanta, U.; Das, S.; Mandal, D.; Sahoo, T.R.

Details: Issue 56, December 2025

Abstract: This study reports the green synthesis of cerium oxide (CeO_2) and magnesium-doped cerium oxide (Mg-doped CeO_2) nanoparticles by a sol–gel method using kiwi (Actinidia deliciosa) peel extract as a natural reducing and stabilizing agent. The synthesized nanoparticles were thoroughly characterized using a range of techniques including XRD, FTIR spectroscopy, FESEM, HRTEM, BET analysis, PL spectroscopy, Raman spectroscopy and UV-Vis spectroscopy. These analyses confirmed the successful synthesis of nanoparticles with well-defined crystalline structures and appropriate morphology. The antibacterial potential of the nanoparticles was evaluated against pathogenic bacteria including methicillin-resistant Staphylococcus aureus, Escherichia coli, and Pseudomonas aeruginosa. Results demonstrated that both nanoparticles exhibited significant antibacterial activity, with Mg-doped CeO_2nanoparticles showing the most potent antibacterial activity. The antibacterial activity of Mg-doped CeO_2nanoparticles was evaluated by measuring the zone of inhibition, which was found to be 12 mm for Staphylococcus aureus, 15 mm for Escherichia coli, and 14 mm for Pseudomonas aeruginosa. Compared with the undoped CeO_2nanoparticles, the Mg-doped CeO_2nanoparticles exhibited enhanced antibacterial efficacy, with minimum inhibitory concentration (MIC) values of 62.5 μg $mL^{-1}$for MRSA (S. aureus), 15.63 μg $mL^{-1}$for E. coli, and 15.63 μg $mL^{-1}$for P. aeruginosa. Furthermore, the synthesized Mg-doped CeO_2nanoparticles demonstrated significant biofilm inhibition activity against methicillin-resistant Staphylococcus aureus (MRSA). The observed antibacterial activity was further supported by reactive oxygen species (ROS) generation, indicating ROS-mediated bactericidal action as the underlying mechanism. These findings highlight the potential of Mg-doped CeO_2nanoparticles as effective antibacterial agents, offering a promising approach for the treatment of bacterial infections including those caused by antimicrobial-resistant strains.

URL: https://pubs.rsc.org/en/content/articlelanding/2025/ra/d5ra07686b

SCHOLARLY PUBLICATIONS
School of Applied Sciences
KIIT Deemed to be University

Journal Name: Scientific Reports **IF: 3.9**

Title: Model simulations capture seasonal Arctic Haze and clean-air cycle better than satellite and reanalysis

Author: Swain, B.; Vountas, M.; Singh, A.; Song, R.; Panda, U.; Schellhorn, H.; Andrae, L.; Deroubaix, A.; Lelli, L.; Tandon, A.; Nikumbh, A.; Gunthe, S.S.

Details: December 2025

Abstract: The Arctic is heating far more rapidly than the global mean, and clarifying the influence of aerosols in this intensification demands accurate and reliable observational records. The Arctic exhibits a distinct seasonal aerosol cycle, springtime ”Arctic Haze” with elevated AOD and summertime “Clean Air” with low AOD. Thus, it is critical to evaluate how well various datasets capture this seasonality relative to ground-based observations. This study analyzes spring and summer AOD variability using CAMSRA and MERRA-2 reanalyses, MODIS Terra and Aqua satellite observations, AERONET measurements, AEROSNOW retrievals, and GEOS-Chem model simulations. Results show that satellite-derived and satellite-assimilated reanalyses are far from capturing the expected seasonal Arctic Haze and Clean Air pattern, except at Bonanza Creek and Yakutsk, where anthropogenic pollution alters it. The inability of reanalyses to capture Arctic aerosol seasonality likely stems from the assimilation of satellite retrievals influenced by cloud contamination and surface reflection from snow and ice, as well as inherent biases in the underlying models used to generate these datasets. In contrast, AERONET observations and GEOS-Chem simulations consistently capture Arctic Haze in spring, driven by long-range transport, and Clean Air in summer, associated with efficient wet removal of aerosols. CAMSRA further underestimates emissions from Arctic forest fires and inadequately represents long-range pollution transport. These findings suggest that independent model simulations align more closely with ground-based observations than satellite products or reanalyses, and that adjusting wet-scavenging parameters to fit such reanalyses may misrepresent aerosol processes and their contribution to Arctic warming. Incorporating advanced retrieval algorithms like AEROSNOW into reanalyses offers a pathway to reduce these biases and improve representation of Arctic aerosol seasonality.

URL: https://www.nature.com/articles/s41598-025-29188-8

Journal Name: Dalton Transactions **IF: 3.3**

Title: Structure-directing effect of terephthalate in bridging Zn(II)- and Cd(II)-based coordination polymers towards application in the detection of trace quantities of Pd2+ in aqueous media and their electrical conductivities

Author: Saha, K; Dutta, B; Das, P; Chandra, A; Samanta, A; Jana, SR; Naskar, S; Saha, R; Ray, PP; Sinha, C

Details: Volume 54, Issue 8, December 2025

Abstract: Energy crisis and environmental pollution are two central themes of contemporary research towards achieving sustainable development goals (SDGs). Material chemistry is the chief discipline that can resolve glitches in these areas through the appropriate design of chemical compounds with multifunctional properties. In this regard, two stable coordination polymers (CPs) were synthesised in this work using Zn(ii) (3d10) and Cd(ii) (d10) metal nodes with 1,4-benzenedicarboxylate (bdc2-) as the bridging ligand and monodentate pyridyl-N coordinated 9H-fluoren-2-yl-pyridin-4-ylmethylene-amine (flpy) as the fluorogenic partner. The structures of the polymers [Zn2(bdc)4(flpy)2]n (CP1) and [Cd(bdc)2(flpy)2(H2O)]n(flpy) (CP2) were confirmed via single-crystal X-ray diffraction measurements. In CP1, the paddle-wheel coordination unit [Zn2(bdc)4] was propagated to constitute a 2D polymer, while in CP2, the capped octahedron motif CdN2O5 generated a 1D chain. Both CP1 and CP2 were strongly emissive, and the emission could be quenched selectively by Pd2+ in aqueous solutions in the presence of as many as twenty other metal ions. Pd(ii) is the most toxic in its three oxidation states of 0, II, and IV, and the limit of detection of Pd2+(aq) was 79.1 nM (CP1) and 89.2 nM (CP2), which were much below the toxicity limit of Pd2+ recommended by WHO (the tolerance limit of Pd2+ in water is 3.97-46.98 mu M). Based on the Tauc plots of the ITO/(CP1 or CP2)/Al thin films, the bandgaps were determined as 3.63 eV for CP1 (theoretical value = 3.28 eV) and 3.55 eV for CP2 (theoretical value = 3.21 eV). Moreover, the electrical conductivity values of the Schottky semiconducting devices fabricated using these polymers at ambient conditions were 1.285 x 10-4 (CP1) and 2.399 x 10-4 S m-1 (CP2). Therefore, the application of these two CPs can accomplish sustainability goals for future generations.

URL: https://pubs.rsc.org/en/content/articlelanding/2025/dt/d5dt90031j

SCHOLARLY PUBLICATIONS
School of Applied Sciences
KIIT Deemed to be University

Journal Name: Icarus **IF: 3.0**

Title: Influence of albedo, radiation pressure, oblateness, and dust belt on the stability in the generalized elliptic restricted three-body problem

Author: Prasadu, B.R.; Mia, R.

Details: Volume 446, March 2026

Abstract: In this paper, we investigate the motion of an infinitesimal body in the framework of the modified elliptic restricted three-body problem by taking into account additional forces due to albedo, radiation pressure, the oblateness of the primaries' and the dust belt. We obtain semi-analytical solutions of locations for non-collinear equilibrium points. The positions of non-collinear equilibrium points are shown graphically for different values of perturbation parameters. To investigate the motion of the infinitesimal body, we have chosen three real astronomical systems: the Sun–Mars, Proxima Centauri, and Sun–Saturn. The effects of different perturbation parameters on the position of non-collinear equilibrium points are analysed. The linear stability analysis of equilibrium points is performed by computing the critical mass ratio. Our findings indicate that the stability and instability of non-collinear equilibrium points are influenced by the mass ratio and specific perturbation parameters associated with each system.

URL: https://www.sciencedirect.com/science/article/abs/pii/S0019103525004336?via%3Dihub